Lawrence Berkeley Laboratory
UNIVERSITY OF CALIFORNIA

Materials & Molecular
Research Division

Submitted to the Journal of Applied Physics

A NEW TECHNIQUE FOR OBSERVING THE AMORPHOUS TO CRYSTALLINE TRANSFORMATION IN THIN SURFACE LAYERS ON SILICON WAFERS

B. Drosd and J. Washburn

February 1980

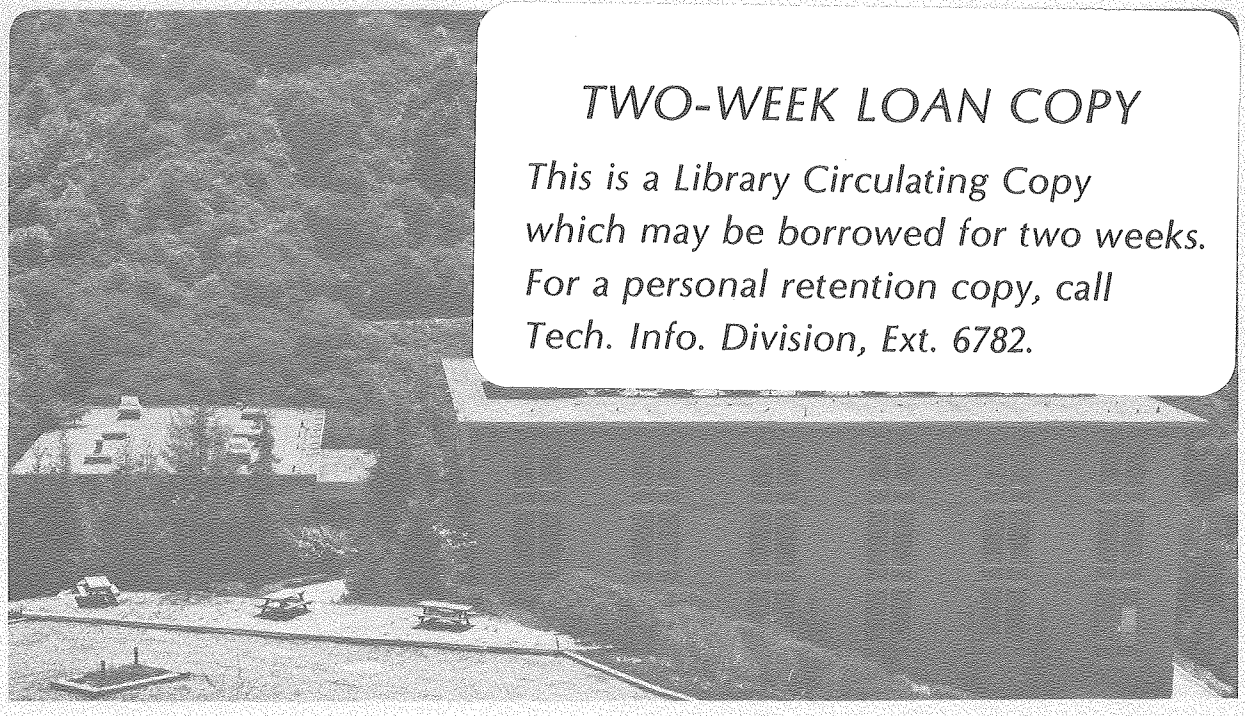

Prepared for the U.S. Department of Energy under Contract W-7405-ENG-48

DISCLAIMER

A NEW TECHNIQUE FOR OBSERVING THE AMORPHOUS TO CRYSTALLINE TRANSFORMATION IN THIN SURFACE LAYERS ON SILICON WAFERS

B. Drosd and J. Washburn

Department of Materials Science and Mineral Engineering
University of California, Berkeley, California 94720

ABSTRACT

Thin amorphous (α) films of silicon created by ion-implantation have been studied in-situ while undergoing the amorphous to crystalline transformation in the electron microscope. The specimens were prepared in such a manner that the amorphous/crystalline interface was viewed edge-on and its advance during annealing was readily observed over distances of several microns. Growth rates and activation energies were measured. The active role that defects play during the regrowth process was also studied. An additional advantage of the technique was that in a single specimen different segments of the recrystallization front advanced along several different growth directions simultaneously, hence the effect of regrowth direction on the interface migration rate and defect formation was graphically displayed in a single specimen.

This work was supported by the U. S. Department of Energy under Contract W-7405-ENG-48

I. INTRODUCTION

High dose ion-implantation of semiconductors may result in the formation of a thin amorphous (α) layer at the implanted surface. The recrystallization process that these layers undergo during annealing is not completely understood[1] but is known to be sensitive to the substrate orientation, implantation temperature, and ion-implanted species among other variables.

Specimens containing thin surface films have been studied by several techniques. Rutherford back-scattering[2] (RBS) measurements have been made which give reasonably good quantitative information concerning the average depth of an α/C interface. However, the RBS technique gives little information about the interface itself or secondary defect formation. Transmission electron microscopy (TEM) analysis is particularly suited for studying crystal defects. Most TEM studies have been made on specimens where the α film plane is perpendicular to the viewing direction as seen in Figure 1. For this case, which will be referred to as a conventional specimen, the defects formed during crystal growth are easily seen and identified, but since they are superimposed on one another, it is difficult to determine the order in which they were formed unless tedious stereo-microscopy or sectioning techniques are employed.[3] At best, quantitative data concerning the regrowth rate of thin α layers would be difficult to obtain by this technique and to our knowledge has not been reported. "Cross-section" specimens[4] have been made for TEM analysis where the α/C interface is seen edge-on. Here the sequence of defect formation has been observed and, in principle, a sequential annealing study could be done. However, the authors are unaware of any such measurements.

A shortcoming of the observation techniques mentioned above lies in the inability to relate the effect of defects in the growing crystal and the interface morphology to measured growth rates. The technique which is described below allows for the simultaneous observation of defects, interface morphology, and rate of interface migration. The present studies were performed on TEM specimens chemically thinned with the α film and specimen plane being parallel, just as for conventional TEM specimens (see Fig. 1). The difference from a conventional specimen lies in the fact that the specimen was thinned prior to annealing. This resulted in an exposed portion of the α layer that was not superimposed on crystalline substrate, as shown in Fig. 2a. Regrowth took place by the motion of the α/C interface from the parent crystal substrate. Homogeneous nucleation of crystallites ahead of the advancing α/C interface was not observed even for long annealing times (similar results[5] have been reported for evaporated α silicon). First, the superimposed α material was consumed after which the interface gradually turned by 90°, from parallel to the specimen plane to approximately perpendicular to it. It then migrated toward the hole in the center of the specimen (Figs. 2b & 2c). At that stage, the interface was sweeping across the field of view. The interface could be observed at different positions around the edge of the hole in the specimen representing regrowth in all the crystallographic directions contained in the plane of the foil. This new type of TEM specimen will be referred to as a thin foil annealed (TFA) specimen. The annealing of silicon thin foil specimens has been attempted by Mazey et al.[6] They observed that the unsupported α material became polycrystalline during annealing.

Occasionally, this was observed in the present work, but only if the specimen was contaminated.

II. EXPERIMENTAL

Amorphous layers were created on the surface of phosphorus doped (5 ohm-cm) silicon wafers by phosphorus ion-implantation to a dose of $10^{16}/cm^2$ at 100kV. The substrate was cooled to 77°K during implantation, using heat conducting paste for good thermal contact with the holder. The ion current was $1\mu A/cm^2$.

For TEM analysis 3 mm discs were cut from unannealed, implanted wafers. They were thinned chemically from the unimplanted side using a nitric/hydrofluoric/acetic acid solution. Annealing of these thinned specimens took place in a tube furnace with a flowing nitrogen atmosphere. Annealing sequences were obtained by repeatedly removing the specimen from the furnace and taking electron micrographs of the same area. The annealing temperatures ranged up to 650°C, above which regrowth occured too rapidly to permit accurate measurements.

III. RESULTS

Crystal growth rates and activation energies have been measured for the <100>, <110>, and <111> growth directions by taking sequential micrographs of the α/C interface during intermittent annealing. Two examples of this are shown in Figure 3 where regrowth in the [100]/(001) and [111]/(1$\bar{1}$0) directions was observed. This notation refers to the [growth direction]/(specimen plane) or GD/SP. In the [100]/(001) case the interface advanced without the formation of any visible defects while for [111]/(1$\bar{1}$0) a high density of microtwins were found. The microstructure resulting from [110]/(1$\bar{1}$0) regrowth was similar to [100]/(001) in that few

defects were observed. These results agree well with those of previous studies of defects in conventional specimens.[7]

The α/C interface, observed during growth in the [100]/(001) and [110]/(1$\bar{1}$0) directions, remained fairly flat for the first micron or two of migration. Beyond this distance the interface became faceted (see the [100] annealing sequence of Fig. 3) and a high density of microtwins was produced during further interface motion, see Fig. 4. Once this had occurred, the growth rate slowed by almost two orders of magnitude. This unusual effect was probably caused by specimen contamination and will be discussed in a later section. All measurements of interface migration rate were confined to the early stages of motion.

The crystal growth rates for the three principal cubic directions were measured and are plotted in Figure 5. Here, it is seen that the activation energy for crystal growth was the same for all directions of growth, 2.9±.1 eV. The <100> growth rate was fastest with the <110> and <111> being 2.3 and 15 times slower, respectively. These relative growth rates agree with previous Rutherford back-scattering studies[1] where the <110> and <111> rates were found to be about 3 and 20 times slower than for the <100>. The activation energy obtained by these previous investigators[8] was 2.4 eV.

The α/C interface will, in general, be curved due to the fact that it bends around the central hole in the specimen formed by chemical thinning. If the curvature is large, many atomic ledges are present on the interface as a geometric necessity and the migration rate during annealing may be affected. The growth rates for [100]/(001) and [110]/(1$\bar{1}$0)

were measured for many speicmens with a wide range of interface curvature. The results are shown in Figure 6 where it is seen that only the [110]/(1$\bar{1}$0) growth direction was curvature sensitive. This result has important implications that will be considered in the discussion.

IV. DISCUSSION

Many of the results obtained from conventional specimens have been confirmed by the present TFA observations. The secondary defect populations resulting from annealing of the [100]/(001), [110]/(1$\bar{1}$0), and [111]/(1$\bar{1}$0) TFA specimens agree well with those found in (100), (110), and (111) conventional specimens, respectively. Twins were found only for the <111> growth directions for both types of specimens. The <100> growth direction produced the fastest growth rate, followed by <110> and <111>, in both the TFA and conventional specimens. However, the crystal growth activation energies were substantially different for the two experiments. The explanation for this difference is not yet clear, but several possibilities exist. The state of stress at the α/C interface in a conventional wafer will be higher since it is constrained in two dimensions, while the TFA specimen is constrained in only one. The higher strain energy in the conventional specimen may supply some of the energy required for atom transfer and therefore reduce the measured activation energy. Another possible reason for the discrepancy is that the α/C interface may be pinned at the two surfaces of the TFA specimen. This would tend to decrease the growth rate and might increase the activation energy.

To obtain the growth rate data shown in Figure 5, only the [100]/(001), [110]/(110), and [111]/(110) GD/SP combinations were used. All others resulted in microtwin formation which would only be expected for regrowth in the <111> direction. This effect is a result of the tendency of the α/C interface to rotate to the lower energy (111) plane. For certain GD/SP combinations the interface can easily rotate to become parallel to (111) as a unit while remaining flat, see Fig. 7c. This can occur in the [110]/(001) and [100]/(011) cases. When the interface can rotate as a unit, it apparently does so immediately since twin formation was observed from the onset of crystal growth. The migration rate for these rotated interfaces was also close to that measured for growth in the <111> direction, as seen in Fig. 5.

In other GD/SP combinations the interface is not able to rotate towards the (111) plane while remaining planar: [100]/(001), [110]/(1$\bar{1}$0), and [110]/(1$\bar{1}\bar{1}$) are examples of this. In this situation, the interface must become faceted in order for (111) growth faces to form, as shown in Fig. 7b. Eventually, this type of faceting did develop, but its formation was always delayed until the interface had moved one or two microns from its initial position. It was during this initial stage of growth that the regrowth microstructures were found to match those for conventional wafers. The growth rate data in Fig. 5 for the <100> and <110> directions was taken well before any faceting began. After faceting occurred, the growth rate slowed by almost two orders of magnitude and a high density of microtwins started to form. The reason for the long delay in facet formation is not yet clear. It was not related to the decrease in foil thickness that occurs as the interface travels

towards the specimen edge. The distance of α/C interface migration prior to formation of facets was found to be approximately the same in many specimens with a wide variety of wedge angles. The most likely possibility is that faceting is associated with an impurity poisoning effect which results from penetration of impurities during annealing. If this were the case, then the interface migration distance before formation of facets may be explained as a result of a balance between the interface migration and impurity diffusion rates.

An additional factor to be considered for the TFA specimens is the curvature of the α/C interface. As mentioned earlier, the [100]/(001) growth rate was unaffected by curvature while the opposite was true for [110]/(1$\bar{1}$0). As explained previously, the latter case actually had a (111) interface. The (111) interface is expected to be atomically smooth[9] and should migrate by nucleation and growth of atomic ledges. If this interface is curved, then it will contain built-in ledges, as a geometric necessity, which will accelerate the crystal growth process. The data in Fig. 6 is consistent with this model. When the radius of curvature was below about 20 microns, a measurable increase in growth rate was observed. However, the effect was easily avoided by using specimens with large central holes.

The role that lattice defects play during recrystallization was also examined using the TFA specimens. The dislocation loops, observed in the conventional (100) and (110) specimens, were seen to form behind the moving α/C interface in a TFA specimen. These loops were a result of the condensation of point defects and were formed after the interface had passed by. In contrast, it appeared that microtwins take an active role

in the α to crystalline transformation. A twin boundary can act as a favorable nucleation site for atomic ledges[10] and can thus accelerate growth on an otherwise smooth surface. Twins at the α/C interface were observed that appeared to be operating in just this capacity, see Fig. 8.

V. CONCLUSIONS

1. Nucleation of the crystalline phase in amorphous silicon is a difficult process. When an amorphous region is in contact with a crystalline region, crystallization takes place entirely by migration of the existing α/C interface.

2. The rate of crystal growth from the amorphous phase is very sensitive to the orientation of the growing crystal face. The fastest rate is for <100> and the slowest is for <111>.

3. The temperature dependence of the growth rate for all faces is the same and corresponds to an activation energy of 2.9±.1 eV for TFA specimens.

4. Microtwin formation occurs only for {111} growth faces.

5. During growth, the faster growing faces tend to disappear leaving only (111) faces.

6. There is a strong possibility that impurity poisoning of {111} growth faces can further reduce the growth rate.

REFERENCES

1. S. Lau, J. Vac. Sci. Tech. 15, 1656, (1978)
2. J. Mayer et al., Can. J. of Phys. 46, 663, (1967)
3. M. Rechtin et al., Phil. Mag. (A) 37, 605, (1978)
4. J. Fletcher, Metals and Materials 7, 530, (1973)
5. N. Blum and C. Feldman, J. Non Cryst. Solids 11, 242, (1972)
6. D. Mazey et al., Phil. Mag. 17, 1145, (1968)
7. R. Drosd, 9th International Congress on Electron Microscopy, p. 384 (ed. J. Sturgess), 1978
8. L. Csepregi et al., J. Appl. Phys. 49, 3906, (1978)
9. K. Jackson, Kinetics of Reactions in Ionic Systems, p. 229, (Plenum Press, 1969)
10. A. Bennett, R. Longini, Phys. Rev. 116, 53, (1959)

FIGURE CAPTIONS

Fig. 1 Schematic drawing of a conventional TEM specimen that was annealed to crystallize the surface amorphous layer prior to chemical thinning.

Fig. 2 Schematic annealing sequence of a wedge shaped specimen (Figure 2a is unannealed). In Figure 2c the regrowth direction is now perpendicular to the original α film plane.

Fig. 3 TEM micrographs of two annealing sequences of TFA specimens. The left column (bright field micrographs) shows regrowth in the [100] direction. Regrowth in the [111] direction (weak beam micrographs) is shown on the right. Annealing times and temperatures are as indicated. [100] regrowth is accomplished without the formation of any visible defects for this short annealing time. A large dirt particle is seen in this sequence which has no effect on the underlying recrystallization process. Interface migration in the [111] direction is accompanied by microtwin formation as seen in the right column.

Fig. 4 Bright field micrograph of a completely annealed (001) TFA specimen that has recrystallized in the [100] direction. The dashed line indicates the original position of the α/C interface. During annealing the α/C interface moved toward the top of the figure for about 1 micron and then became faceted. Beyond this distance, a high density of microtwins was formed during further crystallization. The black dots near, and below, the dashed line are small dislocation loops.

Fig. 5 α/C interface migration rate data for the three principal cubic directions: The fact that [111]/(1$\bar{1}$0) and [110]/(001) recrystallize at the same rate is explained in the discussion section.

Fig. 6 The effect of α/C interface curvature on the growth rate: Only the [110]/(001) growth direction is affected by curvature and then only if the radius of curvature is less than about 20 microns.

Fig. 7 Schematic representation of α/C interface rotation in a wedge-shaped TFA specimen. The upper figure shows the interface prior to rotation. In the lower right a (001) TFA sample is shown recrystallizing in the [110] direction. Here the interface may rotate while remaining planar. In the lower left a (1$\bar{1}$0) TFA sample is shown while recrystallizing in the [110] direction. Here, interface rotation to the {111} planes can only be accomplished by facet formation.

Fig. 8 A bright field micrograph of a (1$\bar{1}$0) TFA specimen recrystallizing in the [111] direction. The three bright elongated objects are microtwins with vertical boundaries with the matrix. The inset diffraction pattern shows the matrix (1$\bar{1}$0) pattern as well as extra spots and streaks indicating that there are plate-like twins present.

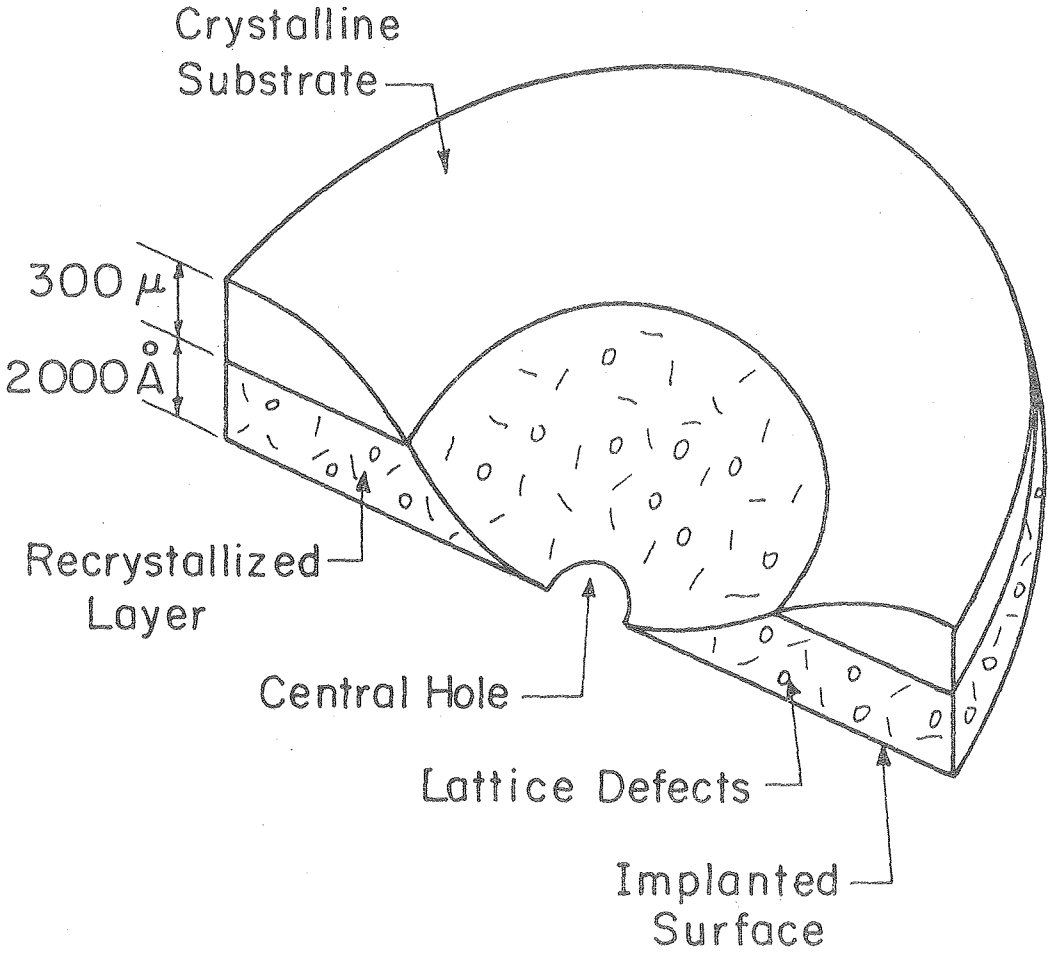
Crystalline
Substrate
300 μ
2000 Å
Recrystallized
Layer
Central Hole
Lattice Defects
Implanted
Surface
XBL7912-14586

Fig. 1

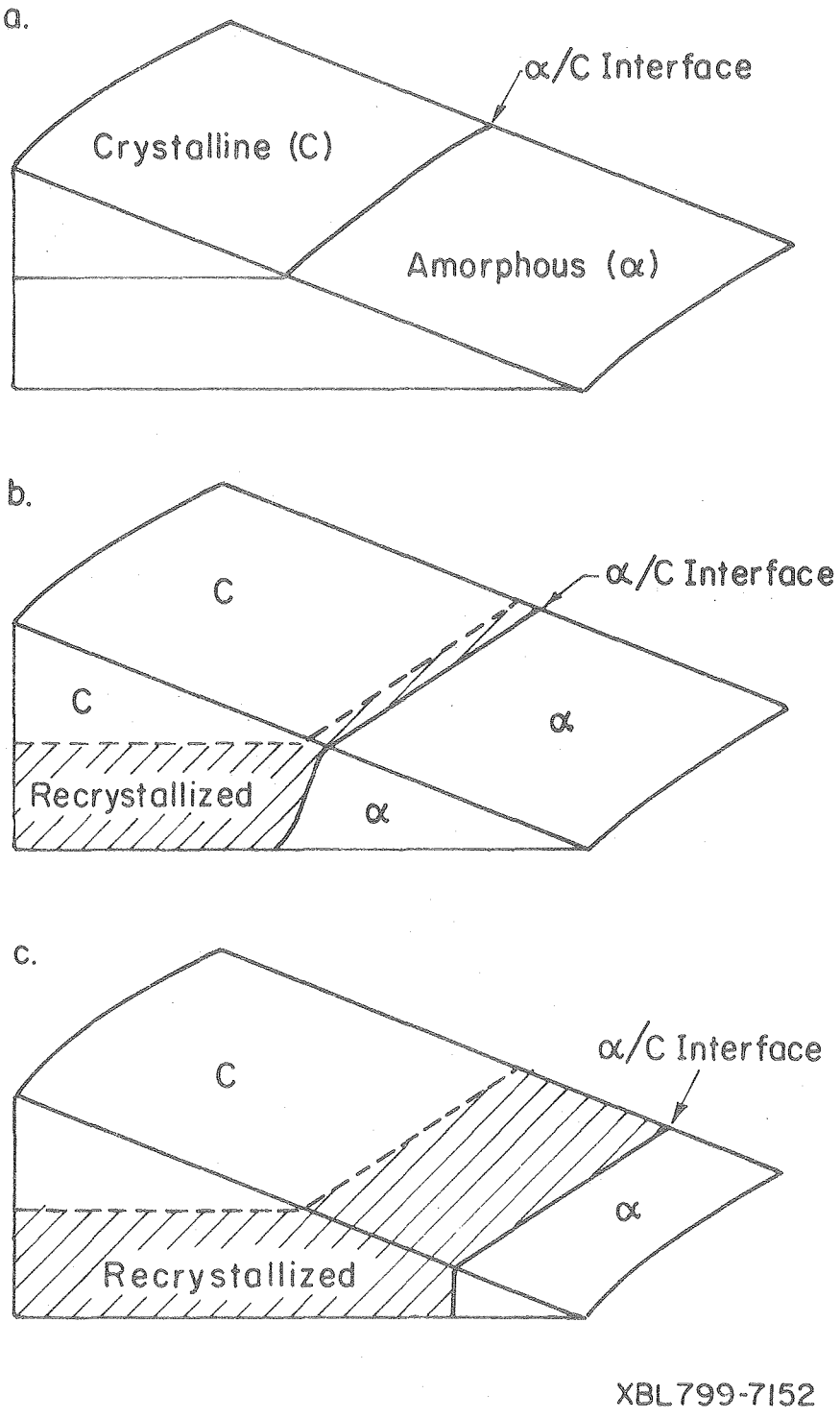
a.
α/C Interface
Crystalline (C)
Amorphous (α)
b.
C
α/C Interface
C
α
Recrystallized
α
c.
C
α/C Interface
α
Recrystallized
XBL799-7152

Fig. 2

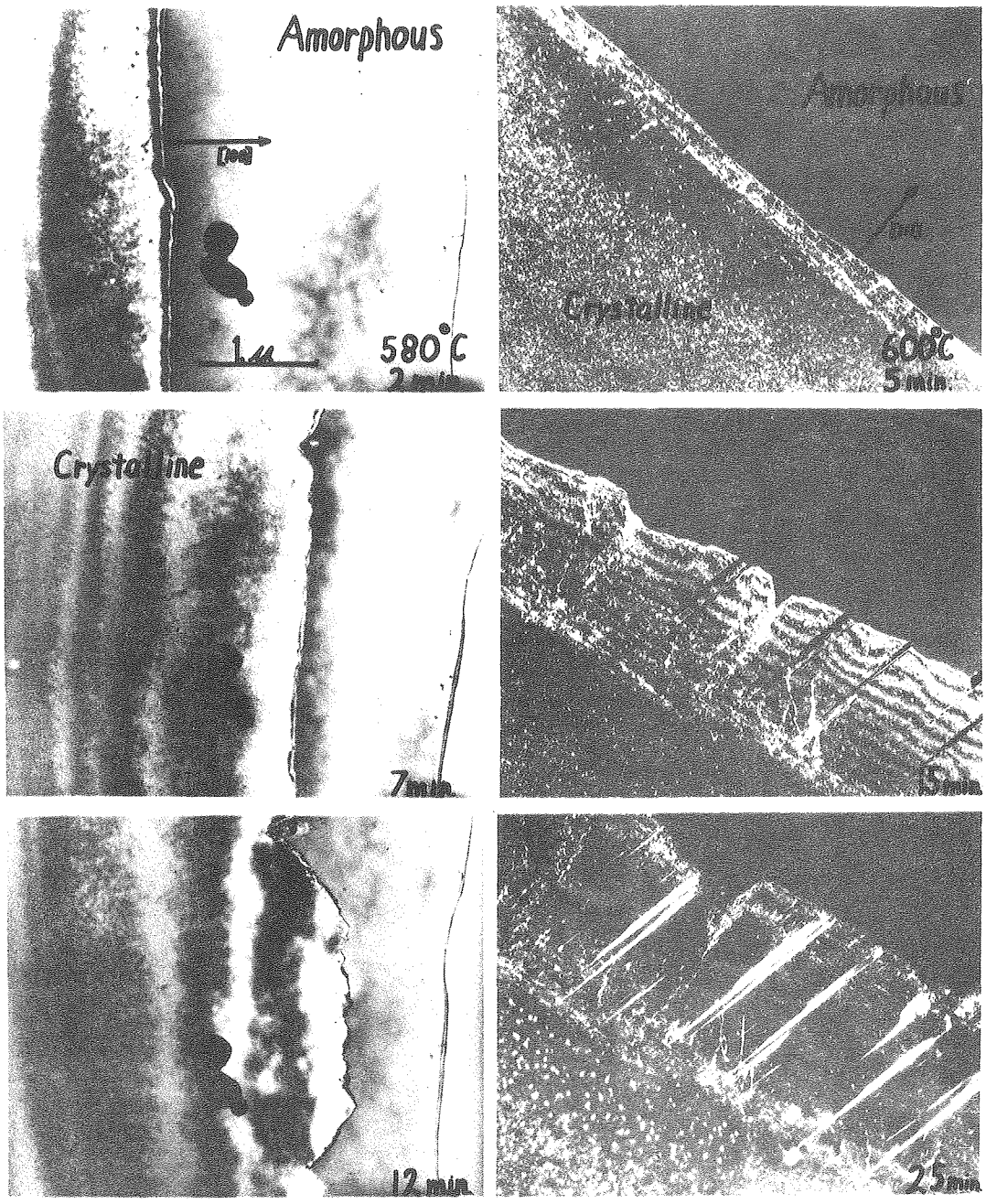

XBB 790-16618

Fig. 3

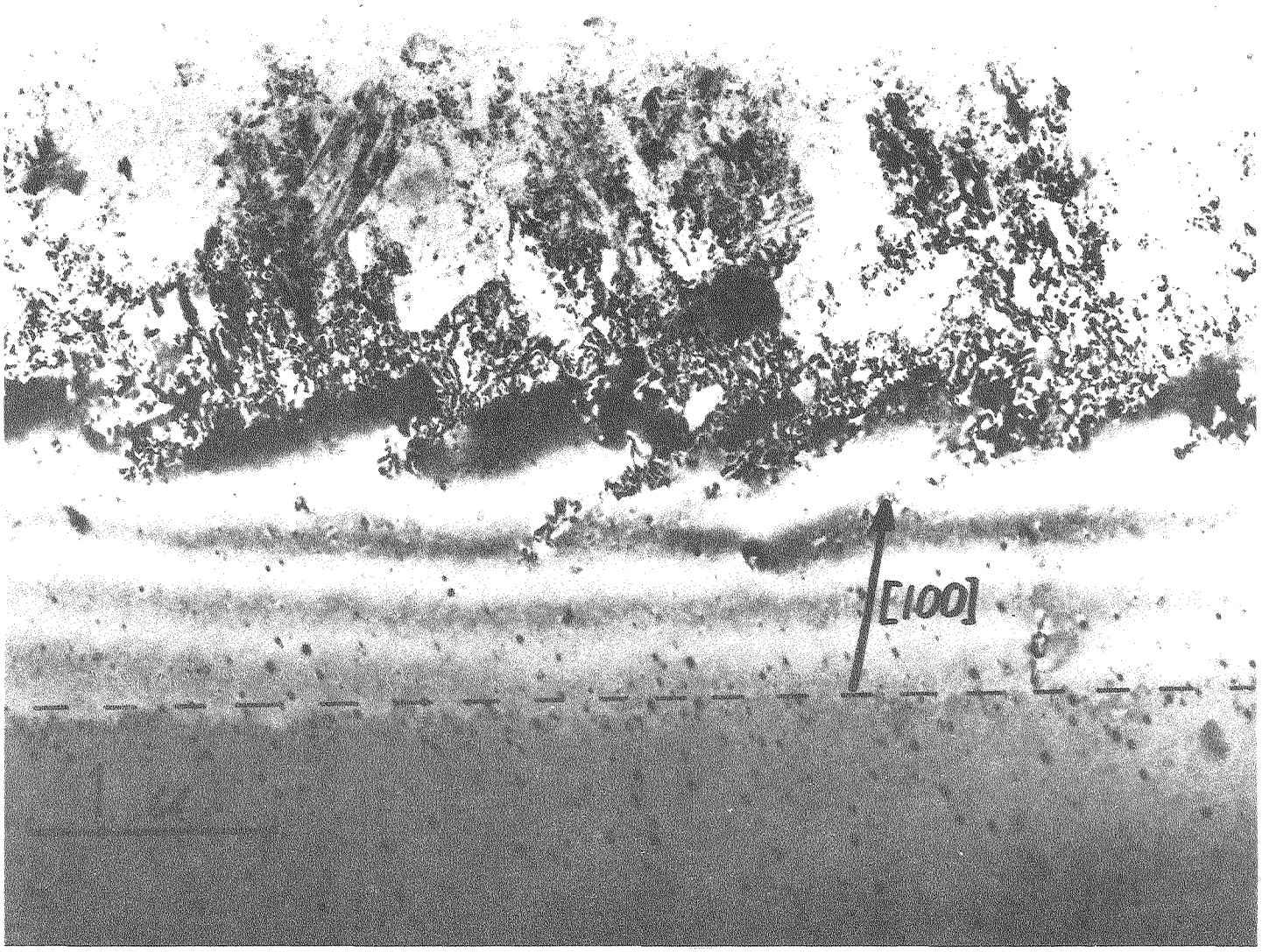

Fig. 4

XBB 790-16064

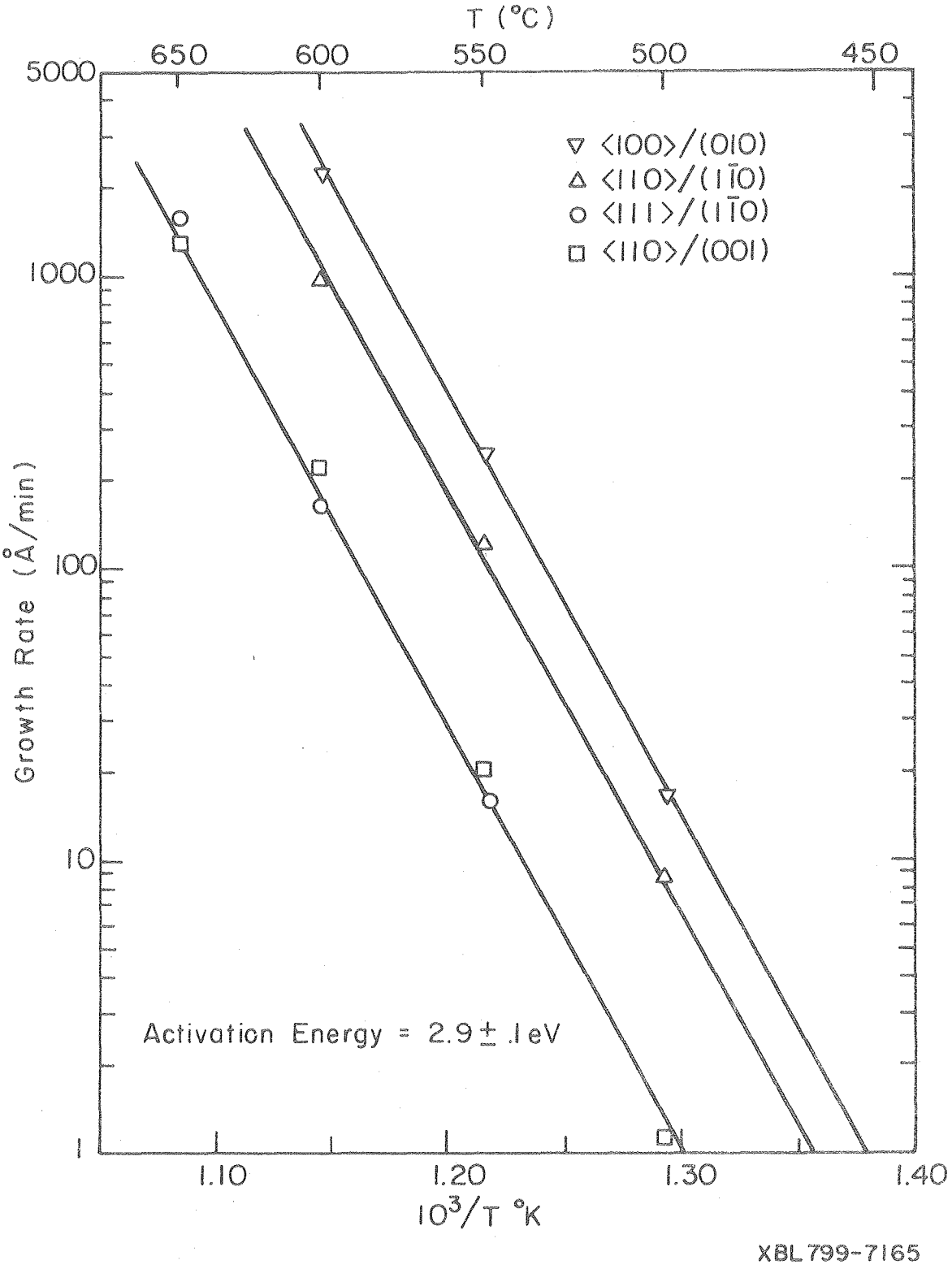
T (°C)
650
600
550
500
450
5000
1000
100
10
1
Growth Rate (Å/min)
▽ <100>/(010)
△ <110>/(1$\bar{1}$0)
○ <111>/(1$\bar{1}$0)
□ <110>/(001)
Activation Energy = 2.9 ± .1eV
1.10
1.20
1.30
1.40
$10^3/T$ °K
XBL 799-7165

Fig. 5

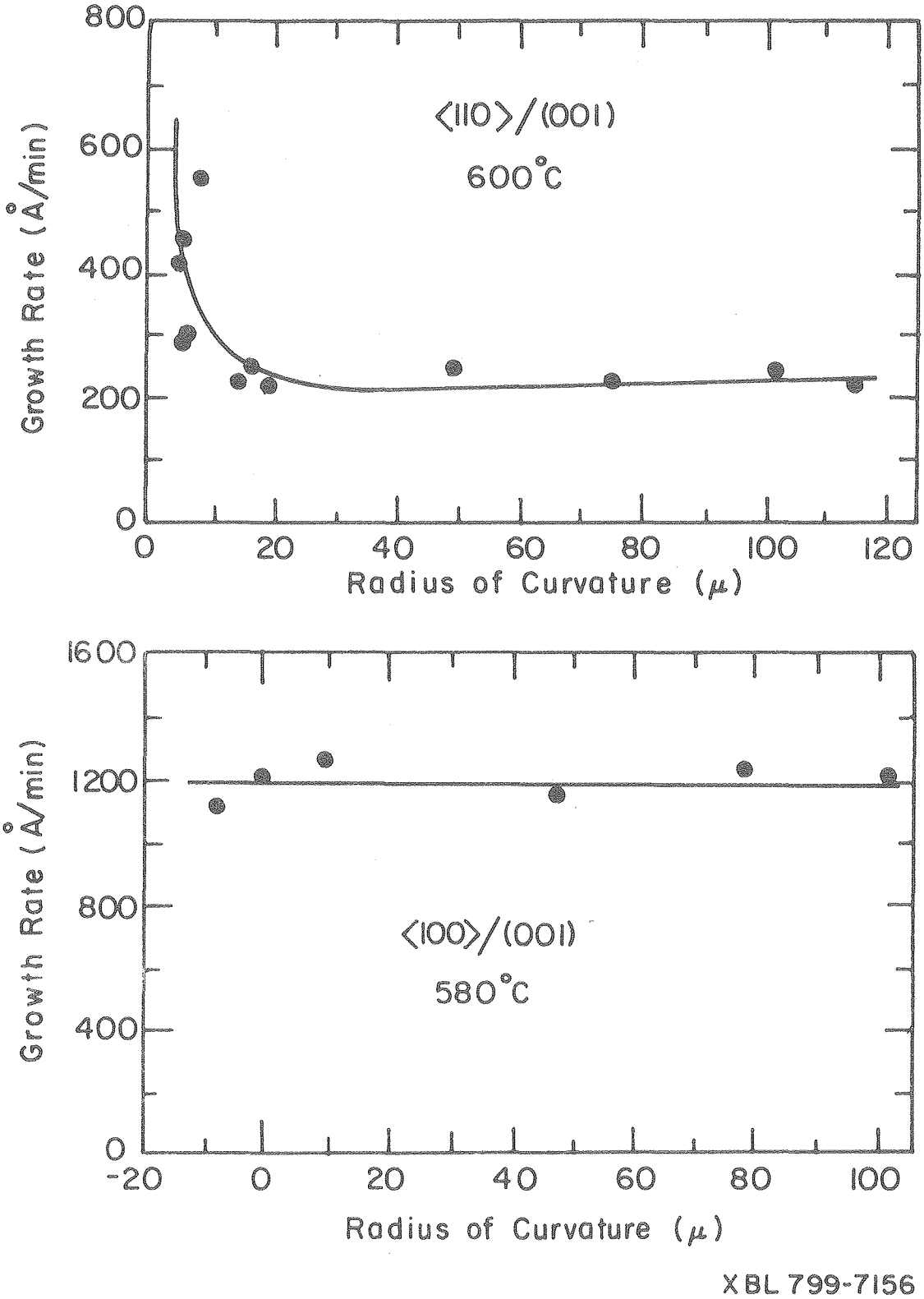
800
600
400
200
0
Growth Rate (Å/min)
⟨110⟩/(001)
600°C
0
20
40
60
80
100
120
Radius of Curvature (μ)
1600
1200
800
400
0
Growth Rate (Å/min)
⟨100⟩/(001)
580°C
-20
0
20
40
60
80
100
Radius of Curvature (μ)
XBL 799-7156

Fig. 6

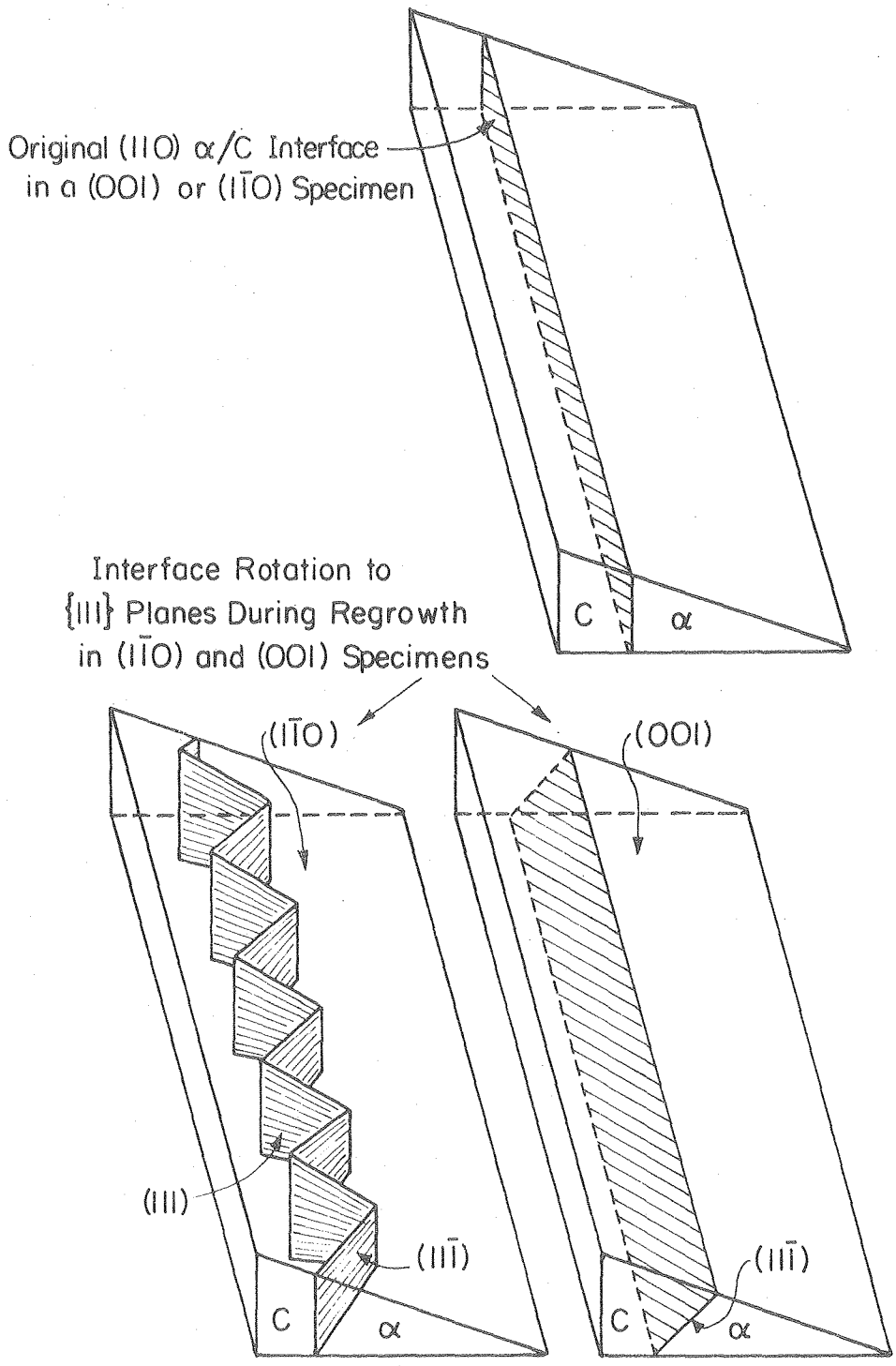

XBL 799-7164

Fig. 7

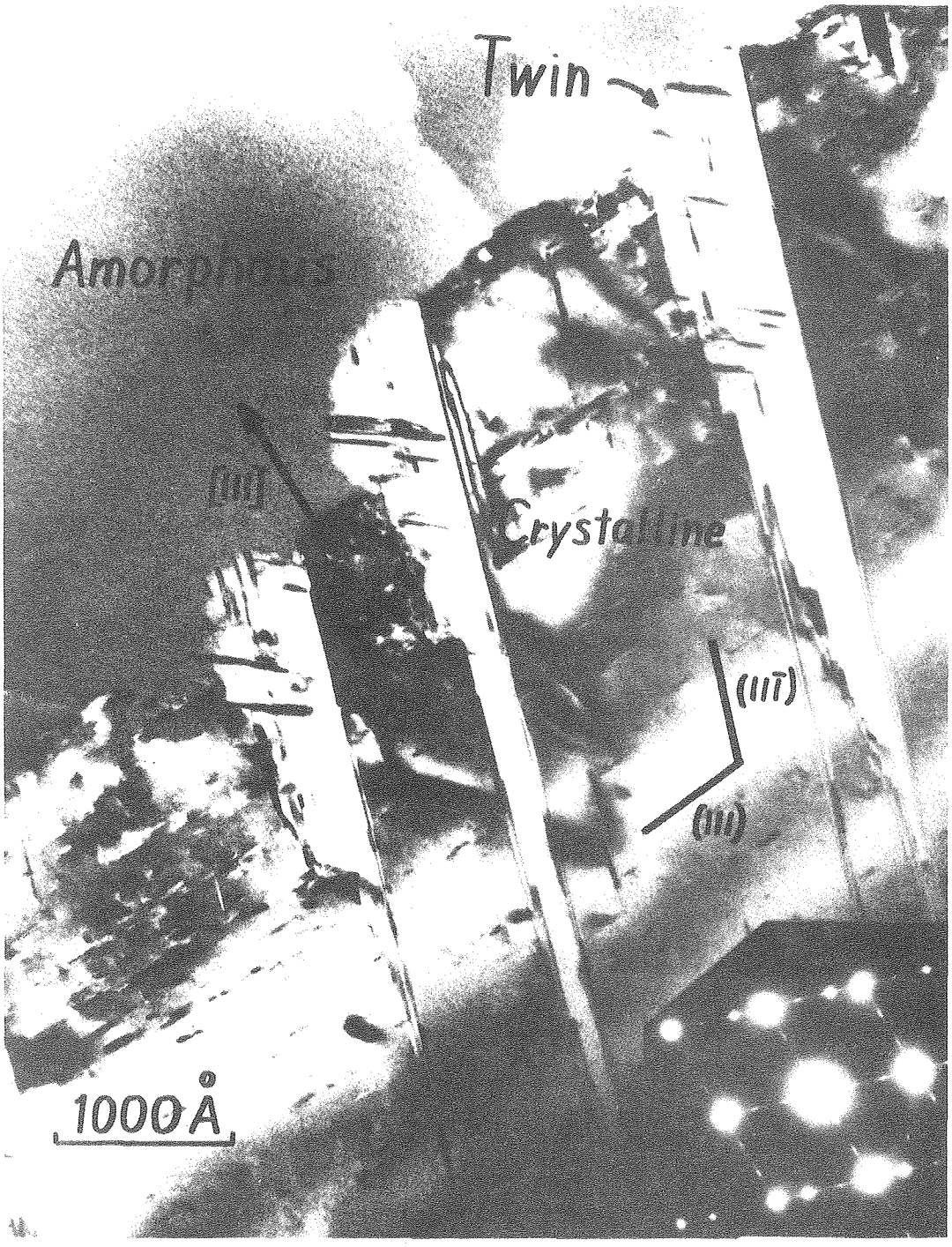

Fig. 8

XBB 790-15623